SHELL GROWTH DYNAMICS IN A CURVED SLAB MOLD AFFECTED BY FLUID FLOW, HEAT TRANSFER AND FLUX INFILTRATION[1]

S. Garcia-Hernandez[2]
J. de J. Barreto[3]
R. D. Morales[4]
J. A. Ramos-Banderas[5]

Abstract

The objective of the present work is to study the effects of the submerged entry nozzle design, steel flow patterns, mold powder infiltration and heat transfer in a curved slab mold on the shell growth dynamics by mathematical simulation. The developed numerical model is based on the solution of the Navier-Stokes equations for incompressible viscous flow, together with the turbulence k-ε model and the Volume of Fluid (VOF) model to solve the multiphase system steel-slag-air. A theoretical approach is used for the heat transfer profiles along the mould walls. The results show that the buoyancy forces have a considerable braking effect on the liquid steel jet velocities and consequently in the flow patterns inside the mold. The mold curvature induces fluid flow patterns variations that have an important influence on the shell growth. And an inappropriate SEN port design has as a consequence that the port is not totally filled by the delivered liquid steel, promoting the formation of a back-flow at the upper edge of the port and also the formation of non-symmetrical oscillating jets. Even when the mold oscillation is not considered, the flux infiltration patterns were homogeneous along the mold and under the simulation conditions did not show to be a variable that affected the shell growth and solidified shell thickness.

Keywords: Shell growth dynamics; Steel flow patterns; Mold powder infiltration; Heat transfer; Mathematical simulation.

[1] *Technical contribution to the 41th Steelmaking Seminar – International, May, 23h-26th 2010, Resende, RJ, Brazil.*

[2] *Graduate Students at the Department of Metallurgy and Materials Engineering, National Polytechnic Institute-ESIQIE, Apdo. Postal 75-874, México City, Mexico. iq_sagahz@hotmail.com*

[3] *Professor, Instituto Tecnológico de Morelia, Metallurgy Graduate Center, Av. Tecnológico No.1500 C.P.58120, Morelia, Mich., México. jbarreto@itmorelia.edu.mx, barretos@prodigy.net.mx*

[4] *Professor at the Department of Metallurgy and Materials Engineering, National Polytechnic Institute-ESIQIE, Apdo. Postal 75-874, México City, Mexico. rmorales@ipn.mx*

1 INTRODUCTION

It is widely known that steel quality depends on a suitable control of turbulent phenomena into the continuous casting mold. Problems like non-metallic inclusions, powder entrapment, steel re-oxidation and non-uniform solidified shell can come up. The most of the studies found in this field are focused on conventional[1-8] and thin slab casting,[9-11] leaving a clear lag in relation to billet and bloom casting. Recently it was shown[12,13] that steel flow dynamics for billet casting is equally complex than that of conventional slabs and then it requires the same attention. Taking into account the late, it is worthwhile to mention that billet mold feeding is carried out by either open stream or Submerged Entry Nozzle (SEN). Fluid flow behavior is far different in both cases and non-studied yet, highlighting a nozzle misalignment due to the manual operation in the actual process. The most of steelmakers that produce very commercial steel rarely use SEN, allowing contact with atmospheric air and subsequent re-oxidation problems. The SEN employment is not the panacea for all casting problems, since a small deviation in its placement could come up free surface instabilities. Also, given the inherent curvature of the continuous casting machines; it is possible to wear the solidified shell in the jet impact zone and a break-out of the line can occur. Thanks to the scarce information about fluid flow behavior into the billet casting mold, the topic represents a great opportunity area to study actual process variables. Major concern in this research are; in one hand, to establish the main differences by using open stream versus SEN and in the other to test ±1 and ±2 degrees of SEN misalignment respect to the exit of the tundish outlet. Variables like turbulence, velocity, wall shear stress, phases behavior (i.e. air-slag-steel) and bath surface oscillations usually the most important to analyze in this process and its relation with the final quality of semi-finished steel products. This is important to point out that fluid flow phenomena in the actual process is extremely difficult to study; owing to that, this study was carried out through mathematical modeling, using real steelmaking data for the simulation process.

2 MATHEMATICAL MODEL

2.1 Fluid Flow and Turbulence Models

The fluid model is based in the solution of the Navier-Stokes equations for compressible viscous flow. The turbulence model was kept as simple as possible without affecting the overall solution. The k-ε model has been proven to give acceptable results in prior works and it is used here to save simulation time. The fundamentals of Navier-Stokes and the k-ε equations can be found easily at many different publication works.[14-17]

2.2 Multiphase Model

The Volume of Fluid (VOF) model was employed to solve the multiphase system air-steel-slag. This scheme performs the calculation of the interface between the phases (*p* and *q*) present at each cell, based on their fraction as shown.[18,19]

$$\rho_{mix} = \alpha_\rho \rho_\rho + (1-\alpha_q)\rho_\rho \qquad \text{and} \qquad \mu_{mix} = \alpha_\rho \mu_\rho + (1-\alpha_q)\mu_\rho \tag{2}$$

A unique continuity equation for the transient system is derived depending on the number of phases; therefore, the Equation 2 is divided by the amount of phase q in

the cell. Mass exchange between phases can be modelled by introducing an additional source term (S_{α_q}).

$$\frac{\partial}{\partial t}(\alpha_q \rho_q) + \nabla \cdot (\alpha_q \rho_q \vec{v}) = S_{\alpha_q} + \sum_{p=1}^{n} (\dot{m}_{pq} - \dot{m}_{qp}) \quad (2)$$

The VOF model solves a single set of momentum transfer equations when two or more phases coexist in the cell.

$$\frac{\partial}{\partial t}(\rho_{mix} v) + \nabla \cdot (\rho_{mix} v v) = -\nabla p + \nabla[\mu_{mix}(\nabla v + \nabla \vec{u})] + \rho_{mix} \beta \Delta T g - S_s + S_\sigma \quad (3)$$

The tracking of the interface is accomplished by an implicit method, which solves the face fluxes ($\dot{m}$) in each grid cell through Equation 4.

$$\frac{\alpha_q^{n+1} \rho_q^{n+1} - \alpha_q^n \rho_q^n}{\partial t} V + \sum_f \left(\rho_q^{n+1} U_f^{n+1} \alpha_{q.f}^{n+1}\right) = \left[S_{\alpha q} + \sum_{p=1}^{n} \left(\dot{m}_{pq} - \dot{m}_{qp}\right) \right] V \quad (4)$$

2.3 Heat Transfer Model

The steel, slag and air share the energy equation which is written as follow.

$$\frac{\partial}{\partial t}(\rho E) + \nabla \cdot (\vec{v}(\rho E + p)) = \nabla \cdot (K_q \nabla T) \quad (5)$$

For the top mould, bottom mould and the cold face the next boundary condition is considered.

$$-k(T)\frac{\partial T}{\partial y} = 0 \quad (6)$$

For the hot face of the mould the next boundary condition is considered: The heat flux to the mould walls was considered as a function of the mould length and it was constant in all walls. This function was obtained from instrumented moulds as reported by Pinheiro et al.[20] which includes the air and steel zones. This heat flux profile was adjusted by curve fitting techniques according to:

Narrow walls

$$-k(T)\frac{\partial T}{\partial y} = -1*(-138262443.488y^4 + 166188994.144y^3 - 60156791.52y^2 + 8044502.48y + 1160913.88) \quad (7)$$

Wide walls

$$-k(T)\frac{\partial T}{\partial y} = -1*(-120979638.05y^4 + 135028557.74y^3 - 48877393.11y^2 + 6536158.26y + 943242.53) \quad (8)$$

2.4 Solidification Model

The solidification profile is calculated for the slag or the steel phase (p, q) based on an enthalpy method where the liquid fraction is calculated by:

$$f_l = \frac{T_q - T_{q,solidus}}{T_{q,liquidus} - T_{q,solidus}} \quad (9)$$

The heat transfer is modified by the latent heat evolution of the steel and slag during solidification in their respective mushy zones. The temperature variation as a function of the effective thermal conductivity of the phase in question is calculated by:

$$\frac{\partial}{\partial t}(\rho_q E)+\nabla\cdot(\rho_q \vec{v} E)=\nabla\cdot(K_q \nabla T) \quad (10)$$

An enthalpy-porosity technique, that treats the mushy zone as a porous medium, is used to include the velocity sink resulting from the solidification. This sink term reduces the velocity depending on the solidification fraction at each cell as show in Equation 11.

$$S_s=\frac{(1-f_l)^2}{(0.001+f_l^2)}A_{mush}(\vec{v}-v_c) \quad (11)$$

2.5 Model Description

A numerical model based on the commercial software FLUENT® was created for a slab curved mould. Figure 1 shows the dimensions of the model that required a computational meshes with a total of 2 500 000 grid cells in a structured mesh. The inlet velocity is calculated to maintain the desired casting speed at the outlet. A pressure inlet condition is applied at the mould top (P=101325 Pa, T=273 K) to model the effects of a system open to the atmosphere. The slag is supplied at this boundary (as in the real process) by calculating the mass of slag required for good casting practice. To calculate mould flux consumption there are many empirical correlations based on analysis of plant data like, for example, those determined by Kwon et al.,[21] Nakajima et al.[22] and Wolf[23] for slabs and blooms, but the most recommendable for billet casters is that proposed by Ogibayashi[24] which is as follow

$$Q=\frac{0.6}{\mu_{flux} v_c} \quad (12)$$

To calculate mould flux viscosity there are also many models such as those of Riboud,[25] Rist,[26] Koyama,[27] Urbain as is explained by Mills[28] and Iida models.[29] The materials properties of the considered phases (Figure 2) and the casting conditions employed on the simulations are presented in the Table 1 and Table 2. This system is initially solved under isothermal conditions until a stable flow pattern is reached after approximately 600 seconds of computational real time. Subsequently, the heat transfer in the system is solved until a uniform temperature field is obtained approximately after 300 seconds of calculation. Finally, the solidification model was activated and modelled for 400 seconds. Convergence is reached when the residuals are below $1X10^{-4}$ in time steps of 0.01 seconds.

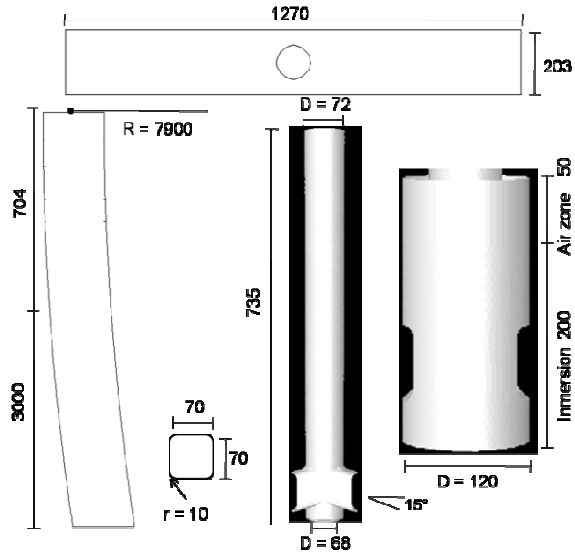

Figure 1. Mold Dimensions (mm).

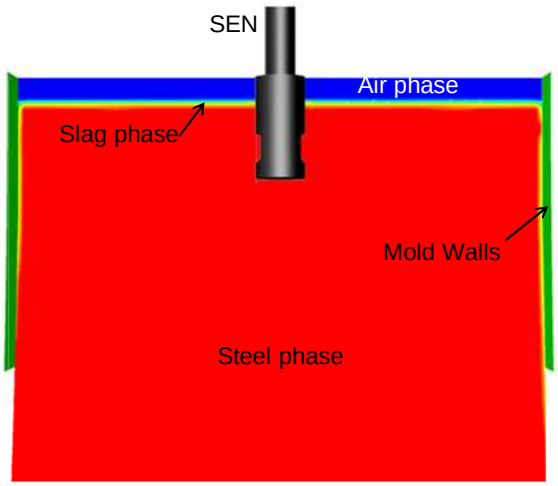

Figure 2. Considered Phases in the Simulation.

Table 1. Thermo-physical properties and parameters used for simulation

Parameters	Values
Casting speed (m/min)	0.9
Nozzle immersion (m)	0.2
Air Zone (m)	0.05
Steel properties*	
Cp (J/kg-K)	720
Thermal expansion coefficient (K^{-1})	0.85358
Thermal conductivity (W m^{-1} K^{-1})	32.7
Density (kg m^{-3})	8586-0.8567 T
Viscosity (Pa s)	0.0064
Melting heat (J kg^{-1})	250,000
Liquidus temperature (C) (30)	1523.435
Solidus temperature (C)	1498.28
Air properties	
Thermal conductivity (W m^{-1} K^{-1})	0.06
Density (kg m^{-3})	1.225
Viscosity (Pa s)	1.789 x 10^{-5}

*Steel chemistry in mass %: C = 0.07, Mn = 0.94, Si = 0.17, V = 0.03, Cb = 0.046, Ca = 0.03, Al = 0.03 and Cu = 0.23.

$$T_{liquidus} = 1537 - 88[\%C] - 25[\%S] - 5[\%Mn] - 2[\%Mo] - 4[\%Ni] - 1.5[\%Cr] - 18[\%Ti] - 2[\%V] - 30[\%P]$$

$$T_{solidus} = 1535 - 200[\%C] - 12.3[\%Si] - 6.8[\%Mn] - 124.5[\%P] - 183.9[\%S] - 4.3[\%Ni] - 1.4[\%Cr] - 4.1[\%Al]$$

Table 2. Chemistry and physical properties of mold flux

Chemistry	(mass %)	Properties	Magnitudes
CaO	36.35	Density (kg m^{-3})	2600
Al_2O_3	7.35	Interfacial tension steel-flux (N m^{-1})	1.3
SiO_2	30.26	Cp (J/kg-K)	1200
Fe_2O_3	0.43	Viscosity (Iida model) (Kg/m-s)	0.09
MgO	1.28	Thermal conductivity (W m^{-1} K^{-1})	1.1
Na_2O	4.33	Liquidus temperature (C)	1159.85
C	5.47	Solidus Temperature (C)	1139.85

3 RESULTS AND DISCUSSION

Since the numerical simulation started considering isothermal conditions and later non-isothermal state a result comparison is firstly made in order analyze whether the flow patterns were affected by the buoyancy forces. For this, a plane at the center of the mold was drawn and the velocity vectors were measured, as shown in Figure 3, for both conditions. From this Figure is clear that the global flow patterns in the mold show the common characteristics, such as: a recirculation on the top of each stream and below a low velocity zone near the entry nozzle, an ascending flow from the lower part of the mold towards the tip of the nozzle, the impact zones of the streams to the narrow faces and a retro-flow at the superior part of the ports. However, comparing Figure 3a to Figure 3b it can be seen differences in the flow patterns. The first difference is a clear velocity decrease on the stream to reach the narrow faces of the mold, due to effect the buoyancy forces; consequently, the ascending and descending velocities, responsible for the re-circulations mentioned above, also are diminished. The second difference is in the lower zone of the steel entry stream, during isothermal conditions the lower re-circulations are large, moving a great amount of flow and are totally distorted; and in non-isothermal state these move lower steel volume, show more symmetry and are located much closer to the lower part of the streams, these differences are directly related to the buoyancy forces. The third difference corresponds to the ascending flow that impacts the tip of the nozzle, at isothermal state a huge ascending flow is observed coming from the two large inferior re-circulations, at non-isothermal conditions this flow diminish considerably and it does not comes from the deep of the mold, this phenomenon is due to the reduction of the re-circulations, which is induced by the buoyancy forces. From these observations is made clear that the buoyancy forces play a very important role in the steel behavior inside the mold and they must be considered in this numerical simulations; consequently, ignoring the buoyancy forces effect involve an inaccuracy in the results obtained.

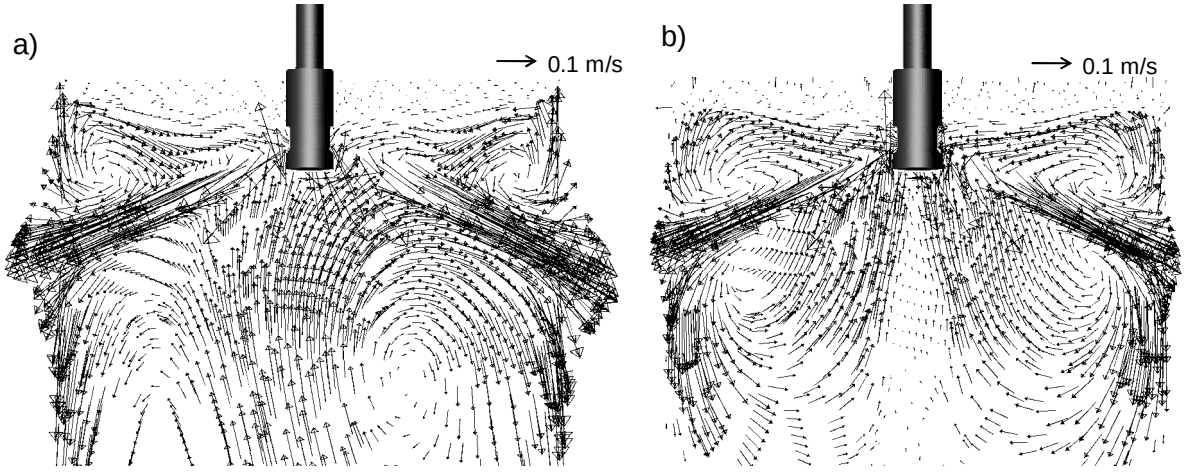

Figure 3. Velocity Vectors at the center of the mold. a) Isothermal and, b) non-isothermal conditions.

In order to evaluate the magnitude of the buoyancy forces and its effect on the inertial forces, a line was drawn at the center of the right hand side entry stream following its trajectory for the cases studied. Along the line the inertial force was measured for isothermal and non-isothermal conditions by $\rho vv/L_0$, from the results

for each condition the differences were calculated, and this was considered as the effect of the buoyancy forces. These results are shown in figure 4, where it can be seen that the effects of the buoyancy forces are very close to cero close to nozzle port and as the stream get away from the port these forces start to increase its magnitude, reaching the highest value at 2/3 of the stream length and then its intensity decreases again close to the mold walls. This figure shows the import role on the flow patterns inside the mold, since they affect considerably the inertial forces of the entry stream.

To observe the balance among the inertial and buoyancy forces on the whole mold, the ratio between these forces was calculated through the following equation[31]:

$$\frac{Gr}{\mathrm{Re}^2} = \frac{0.85358 g \Delta T L}{\rho v^2} \tag{13}$$

The Grashof number was calculated using as reference temperature the average between the mushy and static temperatures of this steel and the results are presented in the central-symmetric plane perpendicular to the mould radius shown in Figure 5.

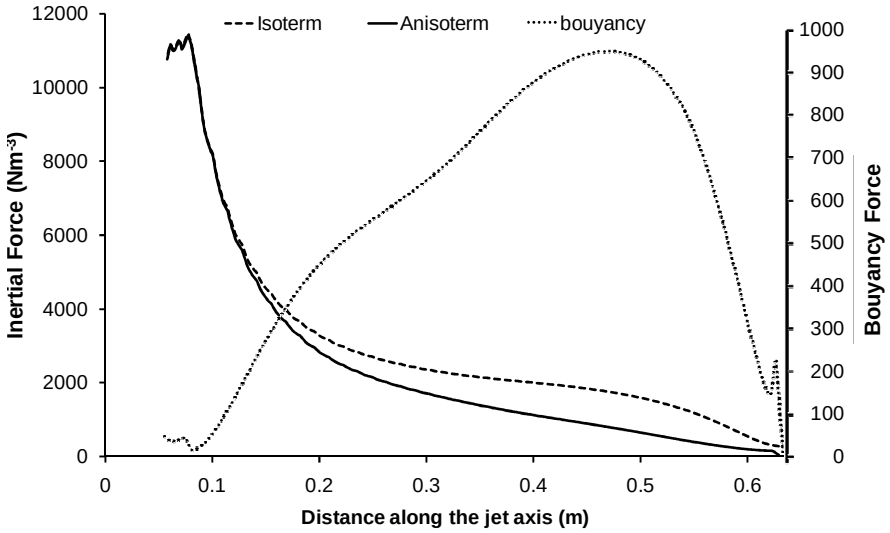

Figure 4. Inertial to Buoyancy Force Balance at the central plane of the right hand side jet.

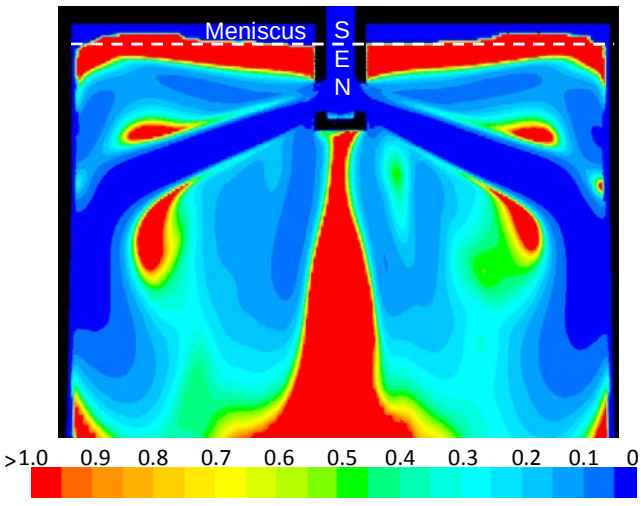

Figure 5. Inertial to buoyancy force balance at the central plane of the mold, after the rate Gr/Re^2.

When this rate tends to cero the inertial forces dominate and when the rate tends to one the buoyancy forces are the dominant over the inertial. From the above figure it can be seen that inside the nozzle and along the stream is where the inertial forces are dominant over the buoyancy ones; however, at the meniscus zones, the recirculation center and the ascending flow towards the tip of the nozzle port is where the buoyancy forces are over the inertial ones, being the dominant forces at these zones. At the rest of the mold the temperature gradients are very variables, as can be seen in Figure 6, for this the rate values among this forces are also very variables making difficult to establish which one dominates over the other; however, it allows to observe a general picture of the force balance and with this conclude that its effect and consideration are definitely transcendental and they must be consider in the simulations of the continuous casting mold.

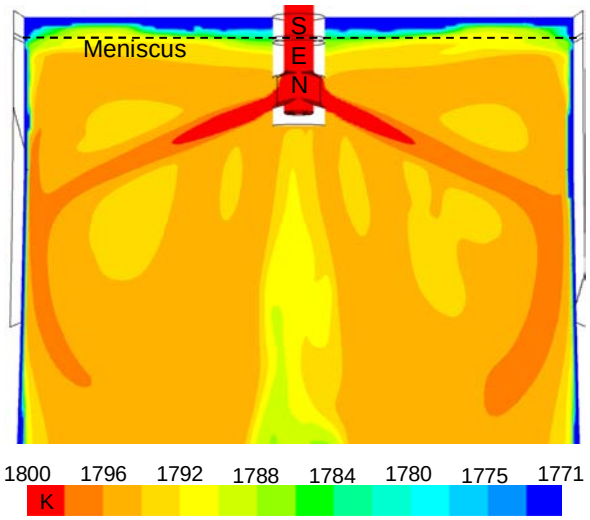

Figure 6. Temperature contours at a central plane of the mold.

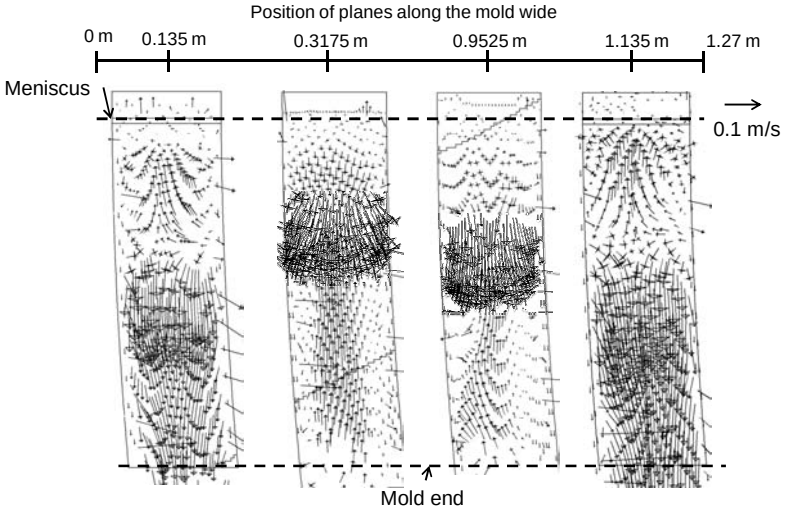

Figure 7. Velocity vectors at 4 planes parallel to the narrow mold face.

Figure 6 shows the temperature contours at the central plane of the mold; taking as a reference the solidus and the superheat temperature, it can be seen that the liquid steel lose its overheat due to the heat extraction at the wide faces of the mold and also the temperature gradients along the mold are considerably different, this changes are more pronounced at the center of the mold. The changes can be attributed to the mold curvature and to the steel re-circulations in that section of the

mold. In order find out the effect of the mold curvature on the flow patterns at non-isothermal conditions, four planes were drawn at 0.13 mm parallel to each narrow face of the mold at which the velocity vectors were determined; these are shown in Figures 7a-7d. These Figures show that the descending steel trajectory after impacting to the faces is slightly different in each plane; in Figure 7a the descending flow shows a tendency to the posterior radius and in Figure 7d the tendency changes to the frontal radius. The planes in Figures 7b y 7c were drawn at the middle distance between the entry nozzle and the narrow faces, it can be seen in Figure 7b that the steel shows a trajectory coming from the posterior radius of the mold and in Figure 7c the behavior is the opposite, indicating that each entry stream feeds the mold wide face differently and when these impact to each other at the center of the mold, having different steel gradients a high heat transfer is taken among the flows, this explains why at the center of the mold the temperature gradients are observed and are so big in comparison to the rest of the mold. Considering the above explanation, it can be expected that the steel solidification along the mold does not be uniform, but it will show strong variations. In order to confirm this hypothesis is correct, four planes parallel to the meniscus were drawn at different mold heights, throughout of the four planes the liquid fractions of steel were acquired, these are shown in Figures 8a-8d; where it can be observed that in some zones the steel has been solidified and the shell thickness is also shown. At the steel level plane, Figure 8a, is observed the start of the solidification and the rest of the steel is still in the liquid state; however, it is important to notice that in the zones between the external nozzle wall and the wide walls of the mold a higher cooling is present comparing to the rest of the liquid zones, this phenomena is the reason for a major growth of the solidified shell at those zones but at deeper levels. Lowering the plane to the tip of the nozzle, Figure 8b, it can be appreciated clearly the zones where the steel streams coming from the entry nozzle crosses this plane and the zones where the liquid steel move upwards once it impact the narrow face of the mold (areas where the liquid fraction is unity), equally it can be observed a solidified shell thickness more delineated but not uniform, mainly at the frontal radius. Going deeper inside the mold, Figure 8c, it is observed the typical thinning of the steel shell at the narrow faces of the mold and the well known thickness increase at the wide faces. Both a related to the flow patterns described previously and shown in Figure 3, the first is due to the washing effect promoted by the stream impact and the second due to the effect of the colder ascending flow near the wide faces of the mold; is very important to stress at this level the irregularities of the shell thickness at the wide faces, but it is most pronounced at the frontal radio. Observing the fourth plane located at the end of the mold, Figure 8d, it was found that the shell thickness at the posterior radio shows a good homogeneity; however, the growth at the frontal radio is totally irregular with a huge number of protuberances, this indicates that since the flow patterns are affected by the mold curvature, the shell thickness and consequently the shell growth is going to be affected and even more at the frontal radio of the mold.

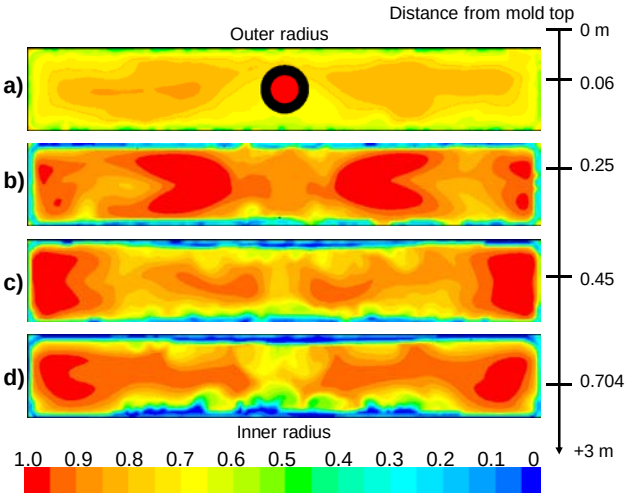

Figure 8. Liquid steel fraction contours at 4 horizontal planes with different metallurgical heights

The above discussion on Figure 8, gave the premise that the solidified steel shell is very variable all along and wide of the mold; however, in order to examine in more details the variations of the solidified steel shell it was necessary to obtain the solidification patterns; these are shown in Figures 9a and 9b. Figure 9a shows a perspective view of the shell growth, in which it can be observed clearly that is in the wide face of the mold where the solidified shell shows the greatest thickness variations, mainly at the center. As explained before, these drastic variations are due to the strong dissimilarity generated by the steel flow at the center of the mold and the excessive growth at the center of the wide face originated from the meniscus, at the zones where it takes place the higher cooling rate. Respect to the narrow faces, Figure 9b, show a close up where it can be observed that the shell growth is definitely much more uniform and that at the level where the stream impact the wall takes place the thinning of the solidified shell. The reason for having a more uniform shell growth can be explained from the much less complexity of the fluidynamics at these faces compared to the wide faces.

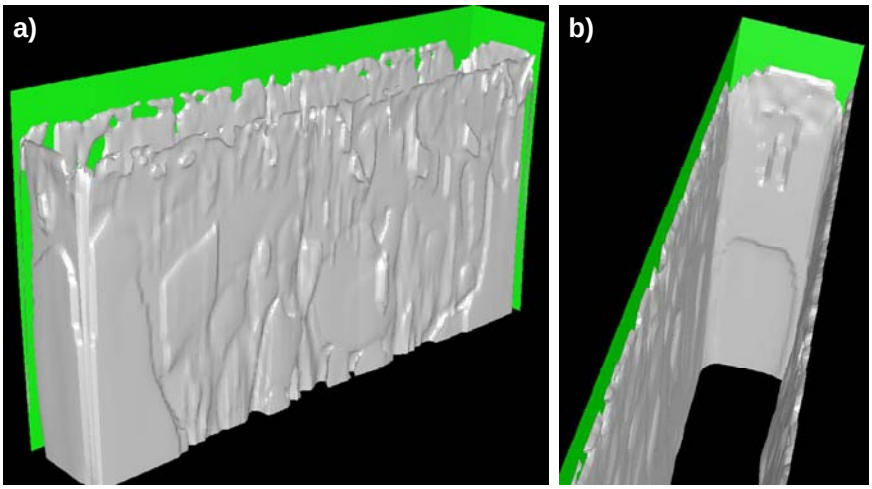

Figure 9. Solidified shell growth: a) Isometric frontal view; b) Thinning view of the shell in a narrow mold face.

Another important factor which also affects the solidified shell is the casting powder. It is well known that if the casting powder does not infiltrate in a uniform manner, the growth of the solidified shell is going to be affected. If there exist a deficiency in the

infiltration of the mold it would be expected a greater shell growth in that face, for this is indispensable to observe the way the powder is infiltrating in that case and determine if this variable is influencing in the irregular growth of the solidified shell. Figures 10a and 10b show the infiltration of the lubricant powder from a frontal view and posterior view in isometric, respectably. From these Figures it can be observed that the powder infiltration is very homogeneous in both faces wide and narrow, this even without considering the mold vibration; is highly probable that if the mold stroke vibration could be considered in the modeling system the infiltration had been much better. However, the results allows to establish that the irregularities found in the solidify steel shell growth were mainly function of the turbulent flow and the casting powder infiltration is homogeneous and good enough that it can be discarded as a transcendental variable under the conditions establish for the system.

So far up to this point, it has been defined that the strong fluid flow fluctuations inside the mold affect considerably the solidify shell growth and that these variations in the fluid flow are in part induced by the mold curvature and the thermal gradients variations. However, is important also important to consider that an inefficient SEN design will affect the flow patterns inside the mold, supplying non-stables and non-symmetric steel streams. In order to observe the flow patterns inside the nozzle, it was taken a plane at the center of the mold and the velocity vectors were acquired making a close up at the port zone of the nozzle, at isothermal and non-isothermal conditions, the results are shown in Figures 11a-11d. Firstly is important to notice is that the port design, even is rectangular induces the formations of a back-flow in the upper part of the port, this is kept for both modeling conditions. This phenomena formation indicated that the port is not totally filled by the leaving steel flow, allowing the formation of the back-flow phenomena. Making a close up to both ports of the nozzle it can be observed that the back-flow shows different intensities between ports, being the left hand side the most intense and keep being even under non-isothermal conditions. This indicates that the nozzle design provide non-symmetric jets, for this reason nozzle design is an important variable that affects the fuidynamics along the mold and should be considered in all the studies that persuade the elimination or reduction the turbulent phenomena found in this work. It is also important to state that the buoyancy forces do not affect the phenomena and the variations of the back-flow developed at the nozzle ports.

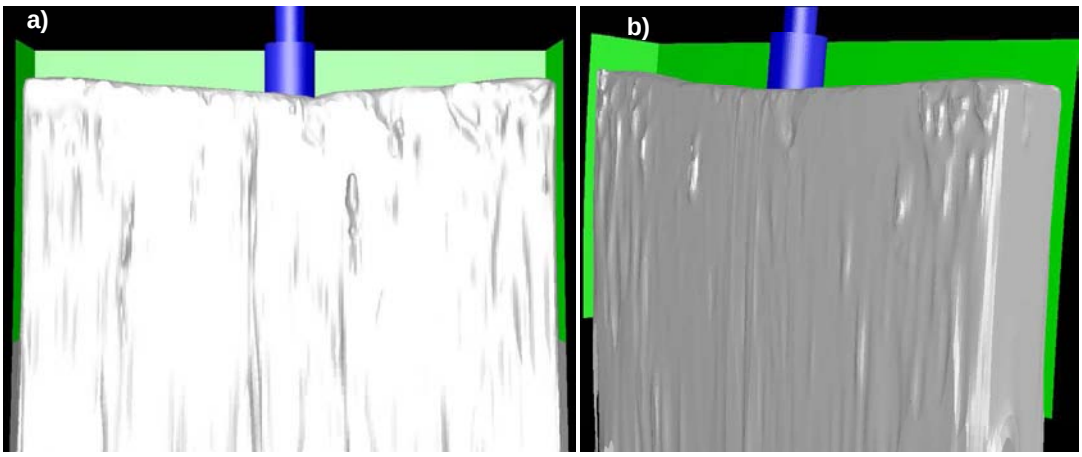

Figure 10. Casting powder Infiltration: a) Frontal view; b) Posterior view in isometric.

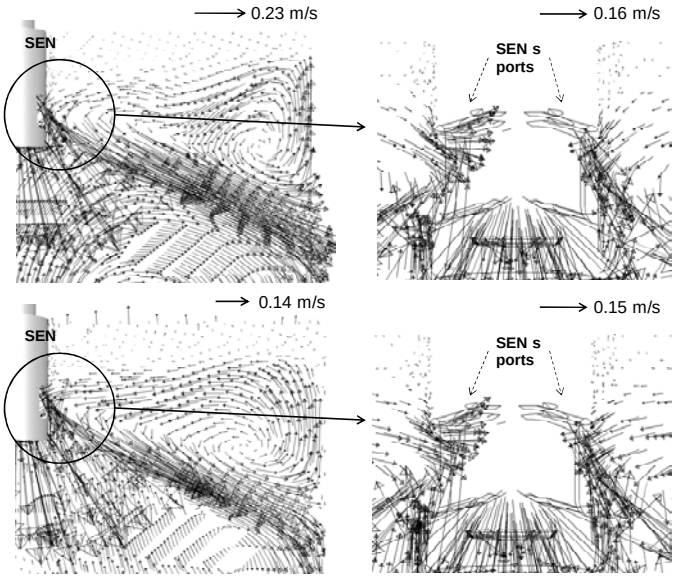

Figure 11. Velocity Vectors at the center of the mold with a close up to the nozzle ports. Isothermic (a y b), non-isothermic (c y d).

4 CONCLUSIONS

The effects of the fluidynamics, the heat transfer and the casting powder infiltration inside the mold on the shell growth dynamics were numerically studied and the main conclusions drawn are as follows:

The buoyancy forces have a considerably effect on velocity break of the entry steel jets and consequently the flow patterns along the mold.

The mold curvature showed to affect the flow patterns of the steel flow and consequently the solidified shell growth, promoting a more uniform growth at the posterior radio than in the frontal one. The growth of the solidified steel shell is lower at the narrow faces due to the thinning induced by the effect of the entry steel jets.

An inefficient nozzle port design has as a consequence that the port is not totally filled by the delivered liquid steel, promoting the formation of a back-flow at the upper edge of the port and also the formation of non-symmetrical oscillating jets.

Even when the mold oscillation is not considered, the flux infiltration patterns were homogeneous along the mold and under the simulation conditions did not show to be a variable that affected the shell growth and solidified shell thickness.

Nomenclature:

E: Enthalpy (J)

f_l: Liquid fraction in the q-phase mushy zone

g : Gravity force (m/s^2)

K_q: Thermal conductivity (W/m s)

k : Turbulence kinetic energy (m^2/s^2)

L : Characteristic length (m)

L_0: Distance from SEN tip to mold end (m)

$\dot{m}_{pq}$, $\dot{m}_{qp}$: Mass transfer from phase to phase

p: Pressure (N/m^z)

p, q: Phases present at each cell

T : Temperature (K)

$T_{liquidus}$, $T_{solidus}$: Liquidus and solidus temperatures (K)

$\vec{v}$, $\vec{u}$ = Fluid velocity (m/s)

U_f : Volume flux throught the face

V : Volume of cell (m^3)

Greek symbols

$\alpha_{p.q}$: Phase fraction

β : Thermal expansion coefficient (1/T)

ε : Turbulence dissipation rate (m^2/s^3)

S_{α_q} : Source term for mass exchange

S_s : Momentum sink due to the solidification

S_σ : Source term due to the surface tension

ρ_{mix} , $\rho_{p,q}$: Mixture and phase densities (Kg/m^3)

μ_{mix} , $\mu_{p,q}$, μ_{flux} : Mixture, phase and mold powder viscosities (N-s/m^2)

REFERENCES

1 S. Ramirez-Lopez, R.D. Morales, A. Najera-Bastida, J. Palafox-Ramos, L. Garcia-Demedices, O. Davila: *Metall. Mater. Trans.* B, **36**, 6, (2005), pp.787-800.

2 A. Ramos-Banderas, R. Sánchez-Pérez, R.D. Morales, J. Palafox-Ramos, L. Demedices-Garcia and M. Díaz-Crúz: *Metall. Mater. Trans.* B, **35**, 3, (2004), pp.449-460.

3 A. Ramos-Banderas, R. Sánchez-Pérez, R.D. Morales, J. Palafox-Ramos y L. García–Demedices, Canadian Metallurgical Quarterly, **43**, 3, (2004), pp.329-338.

4 K. Takatani, Y. Tanizawa, H. Mizukami, and H. Nishimura,ISIJ Int., **41**, 10, (2001), pp.1252-1261.

5 R. Sanchez-Perez, R.D. Morales, M. Díaz-Cruz, O. Olivares –Xometl y J. Palafox-Ramos, ISIJ Int., **43**, 5, (2003), pp.637-646.

6 R. Sanchez-Perez, R.D. Morales , A. Ramos-Banderas and J. Palafox-Ramos, Steel Grips., **2**, 1, (2004), pp. 57-65.

7 B.G. Thomas, X. Huang and R.C. Sussman: *Metall. Mater. Trans.* B, **25**, (1994), pp.527-547.

8 Y.H. Ho, C.H. Chen y W.S. Wang, Ironmaking and Steelmaking, **28**, 3, (2001), pp.258-265.

9 E. Torres-Alonso, R.D. Morales, L.G. Demedices, Alfonso Najera, J. Palafox-Ramos, P. Ramirez-Lopez, ISIJ Int., **47**, 5, (2007), pp.679-688

10 N. Hoseok, P. Hwa-Soo, J. K. Yoon, ISIJ Int., **40** , 9, (2000), pp.886-892

11 T. Honeyands, J. Herbertson: Steel Research Int., **66**, 7, (1995), pp.287-293

12 R. Saraswat, D. M. Maijer, P. D. Lee, K. C. Mills, ISIJ Int., **47**, 1, (2007), pp.95-104.

13 E. Torres-Alonso, R.D. Morales, S. Garcia-Hernandez, A. Najera-Bastida, A. Sandoval-Ramos: *Metall. Mater. Trans. B*, **39**, 6, (2008), pp.840-852.

14 B. Zhao, B.G. Thomas, S.P. Vanka and R.J. O´Malley: *Metall. Mater. Trans.* B, 36 (2005), 801.

15 R.D. Morales and P. Ramirez-Lopez: Proc. AISTech Conf., 20 (2006).

16 R.D. Morales: Proc. 15th Steelmaking Conf., Instituto Argentino de Siderurgia, Sn. Nicolás Argentina (2005), 253.

17 S. B. Pope: Turbulence Flows, Cornell University, Cambridge University Press, (2000).

18 Fluent Documentation, Fluent Inc., Lebanon NH, USA, (2007).

19 J. Liow, L. Rudman and P. Liovic: *ISIJ Int.*, 41 (2001), 225.

20 C. A. M. Pinheiro, I. V. Samarasekera, J. K. Brimacombe, B. Howes and O. Gussias: *Ironmaking and Steelmaking*, **27** (2000), 144.

21 O.D. Kwon, J. Choi, I.R. Lee, J.W. Kim, K.H. Moon and Y.K. Shin: Steelmaking Conf. Proc., ISS, (1991), 561.

22 K. Nakajima, H. Hiraki, T. Kanazawa and T. Murakami: *CAMP-ISIJ,* **5** (1992), 1221.

23 M.M. Wolf: *Trans. ISIJ*, **20** (1980), 718.

24 S. Ogibayashi: Nippon Steel Technical Report, **34** (1987), 1.

25 A.S. Normanton, V. Ludlow, B. Harris, M. Hecht, C.A. Dacker, A.Di Donato and T. Sohlgren: Mould Powder Consumption, Melting and Lubrication and their Effects on Mould Heat Transfer and Subsequent Surface Quality of Continuously Cast Slab, Technical Steel Research, (2005), 116.

26 W. Kim, J. Choi, O.C. Kwon, R.I. Lee, Y.K. Shin and J.S. Park: Proc. of 4th Int. Conf. on Molten Slags, Fluxes and Salts, (1992), 468.

27 K. Koyama, K. Nagano, Y. Nagano and T. Nakano: Nippon Steel Technical Report, **34** (1987), 41.

28 K.C. Mills and B.J. Keene: *Int. Mater. Rev.*, **32** (1987), 2-229.
29 T. Iida, H. Sakai, Y. Kita and K. Shigeno: *ISIJ Int.*, **40** (2000), S-110.
30 J.M. Cabrera-Marrero, V. Carreño-Galindo and R. D. Morales: *ISIJ Int.*, **38** (1998), 822.
31 S. Joo, J. W. Han and R. I. L. Guthrie: *Metall. Mater. Trans. B*, **24** (1993), 767.